

Raman scattering in a GaAs/Ga_{1-x}Al_xAs Fibonacci superlattice

D. J. Lockwood, A. H. MacDonald, G. C. Aers, M. W. C. Dharma-wardana,
R. L. S. Devine, and W. T. Moore

Division of Physics, National Research Council, Ottawa, Canada K1A 0R6

(Received 18 May 1987)

Raman scattering from acoustic phonons in a GaAs/Ga_{1-x}Al_xAs Fibonacci superlattice is reported. Peaks are observed at a set of frequencies that are found to be in good agreement with theoretical predictions based on an elastic continuum model. The influence of the internal structure of the Fibonacci sequence elements and of the mixing of phonon modes on the weights and positions of spectral features is discussed. A simple expression is derived that provides an upper bound on gaps in the phonon spectrum resulting from the quasiperiodic structure.

The discovery of quasicrystals^{1,2} has stimulated interest in the physical properties of systems with quasiperiodic order. Naturally occurring quasicrystals have complicated structures³ and their properties may be difficult to understand in detail. It is clear that comparison of experiments on artificially fabricated quasiperiodic structures with theory has some advantages and will play an important role in the development of this subject. This approach was first suggested by Merlin *et al.*⁴ who fabricated a Fibonacci sequence of semiconducting layers (see below) and measured the x-ray diffraction pattern^{4,5} and Raman spectra.⁴ More recently the properties of quasiperiodic superconducting multilayer systems⁶ and two-dimensional networks⁷ have been studied. Here we present Raman spectra for a Fibonacci superlattice composed of layers of GaAs and Ga_{1-x}Al_xAs ($x \approx 0.25$) grown by molecular-beam epitaxy that are in good agreement with theoretical predictions based on an elastic-continuum model for acoustic phonons. The spectra differ qualitatively from those reported in Ref. 4 but are similar to and have the same interpretation as those reported for Si/Si_{1-x}Ge_x Fibonacci superlattices by Dharma-wardana *et al.*⁸ Similar data for the GaAs/AlAs Fibonacci superlattice of Ref. 4 have recently been reported by Bajema and Merlin,⁹ who point out that a qualitative change occurs when the Raman spectrum is recorded with excitation on an electronic resonance, as was the case with the original experiment. Our data, taken on a sample with very similar compositional geometry, only partially support their interpretation of the on-resonance spectrum. However, although some of our spectra were taken at the same excitation wavelength (647.1 nm) as in Ref. 4, we did not determine if exact resonance was actually achieved at this wavelength.

The GaAs-Ga_{1-x}Al_xAs Fibonacci superlattice was grown by molecular-beam epitaxy on a GaAs(100) substrate at a temperature of 650°C. A Fibonacci superlattice comprises an arrangement of layers of type *A* and type *B* following the Fibonacci sequence $S_1 = A$, $S_2 = AB$, $S_3 = ABA$, \dots , $S_j = S_{j-1}S_{j-2}$. The *j*th-generation superlattice consists of F_j *A* intervals and

F_{j-1} *B* intervals, where $\{F_j\}$ are the Fibonacci numbers defined iteratively by $F_j = F_{j-1} + F_{j-2}$, for $j \geq 2$, with $F_0 = 0$ and $F_1 = 1$. For growth purposes, the intervals *A* and *B* were subdivided into a GaAs layer of thickness d_1^A and d_1^B , respectively, plus a Ga_{0.75}Al_{0.25}As layer of thickness d_2 . Previous calibrations of growth rates resulted in the following estimates of layer thicknesses: $d_1^A = 18$ monolayers, $d_1^B = 8$ monolayers, and $d_2 = 8$ monolayers, with one monolayer corresponding to a thickness of 2.82 Å. A 13th generation superlattice was grown with these building blocks and it had a total thickness of approximately 2.3 μm. Thus the approximate widths of the *A* and *B* intervals are $d_A = d_1^A + d_2 = 73.3$ Å and $d_B = d_1^B + d_2 = 45.1$ Å, respectively, and the quasiperiodicity is characterized by the length $d = \tau d_A + d_B$, where the golden mean $\tau = (1 + \sqrt{5})/2$.

The Raman spectrum of the sample placed in a He-gas atmosphere at 295 K was measured in a 90° scattering geometry with the (100) surface inclined at an angle of 12° to the incident light. The spectrum was excited variously with 300 mW of 457.9-nm Ar-laser light and of 647.1-nm (and 676.4-nm) Kr-laser light, analyzed with a Spex 14018 double monochromator, and detected with a cooled RCA 31034A photomultiplier. The large refractive index of GaAs at these laser wavelengths makes the experiment almost like backscattering within the sample. The photon momentum transfer was deduced from the experimental geometry, the laser wavelength, and the refractive index of GaAs at that wavelength.

Typical Raman spectra are given in Fig. 1 (the spectra obtained with 647.1- and 676.4-nm excitation are very similar). The spectrum recorded under excitation at 457.9 nm shows a series of lines at low frequencies typical of superlattice acoustic modes.^{8,10} The results obtained with red laser excitation appear quite different as the weak Raman spectrum is superimposed on a relatively intense emission spectrum produced by these near-resonance excitation wavelengths. The Raman spectrum is so weak in these cases (the uncorrected 290-cm⁻¹ LO-phonon intensities for 457.9-, 647.1-, and 676.4-nm excitation are in the ratio 11:1:1) that only the most

prominent lines are visible. The near-resonance results are thus similar to those obtained earlier for the GaAs-AlAs Fibonacci superlattice^{4,9} in that a weak Raman spectrum comprising peaks on an underlying continuum is observed, but clearly our spectra cannot be interpreted in terms of dips (rather than peaks) in the continuum created by gaps in the phonon density of states.^{4,9}

The continuum model expression for Raman scattering from acoustic phonons is¹⁰

$$I(\omega) \propto \sum_j \delta(\omega - \omega_j) \times \left| \sum_k (q - k) P(k) u^j(q - k) \right|^2 [n(\omega) + 1] / \omega, \quad (1)$$

where $u^j(q - k)$ is the normalized Fourier transform of the local displacement from equilibrium for the acoustic phonon with frequency ω_j , q is the light wave vector, and $P(k)$ is the Fourier transform of the local photoelastic coupling constant. The phonon frequencies are determined by solving¹¹

$$v^2(\xi) \frac{d^2 u}{d\xi^2} + \omega^2 u = 0, \quad (2)$$

where ξ is the coordinate along the Fibonacci superlattice and $v(\xi)$ is the local sound velocity. $P(\xi)$ and $v(\xi)$ are piecewise constant and u and $du/d\xi$ must be continuous at interfaces. In our case we estimate that $v = 4.72 \times 10^5$ cm/s in GaAs and $v = 4.94 \times 10^5$ cm/s in Ga_{1-x}Al_xAs, while P in GaAs is about 25% larger than in Ga_{1-x}Al_xAs [P in bulk GaAs is ~ 10 times larger than in AlAs (Refs. 10, 12, and 13)].

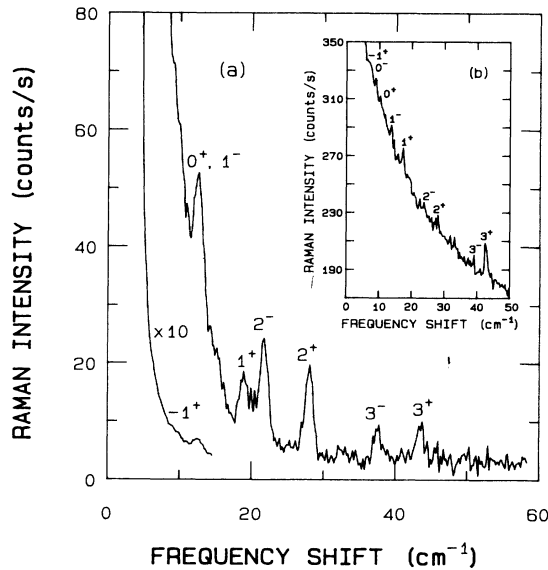


FIG. 1. The unpolarized Raman spectrum of the Fibonacci superlattice recorded at 0.8 cm^{-1} resolution with (a) 457.9-nm and (b) 647.1-nm excitation using spectrometer slit widths of 50 and $100 \mu\text{m}$, respectively. See Table I for the labeling of the peaks.

Because the sound velocities differ far less than the photoelastic constants it is a good approximation to replace the sound velocity in Eq. (2) by its rms spatial average ($\bar{v} = 4.79 \times 10^5$ cm/s). (Corrections are discussed below.) In this case the phonon modes have a single Fourier component and, in the high-temperature limit, Eq. (1) reduces to

$$I(\omega) \propto \sum_k \delta(\omega - \bar{v} |k + q|) |P(k)|^2. \quad (3)$$

Projecting from two dimensions, an expression can be derived for $P(k)$ for an arbitrary Fibonacci superlattice.^{8,14-16} For the case studied here, where d_2 is identical in the A and B intervals of the Fibonacci sequence,

$$P(k) = \sum_{n \neq 0, m \neq 0} \delta(k - k_{n,m}) (P_2 - P_1) S(k_{n,m}) + \delta(k) \bar{P}, \quad (4)$$

where $k_{n,m} = 2\pi(m + n\tau)/d$, \bar{P} is the spatial average of $P(\xi)$, and

$$|S(k_{n,m})|^2 = \left| \frac{2\tau^2 \sin(k_{n,m} d_2 / 2) \sin(Z_{n,m})}{k_{n,m} Z_{n,m} d} \right|^2. \quad (5)$$

In Eq. (5) $Z_{n,m} = \pi\tau[m(d_A/d_B) - n]/(\tau^{-1} + d_A/d_B)$ is proportional to the component of the two-dimensional

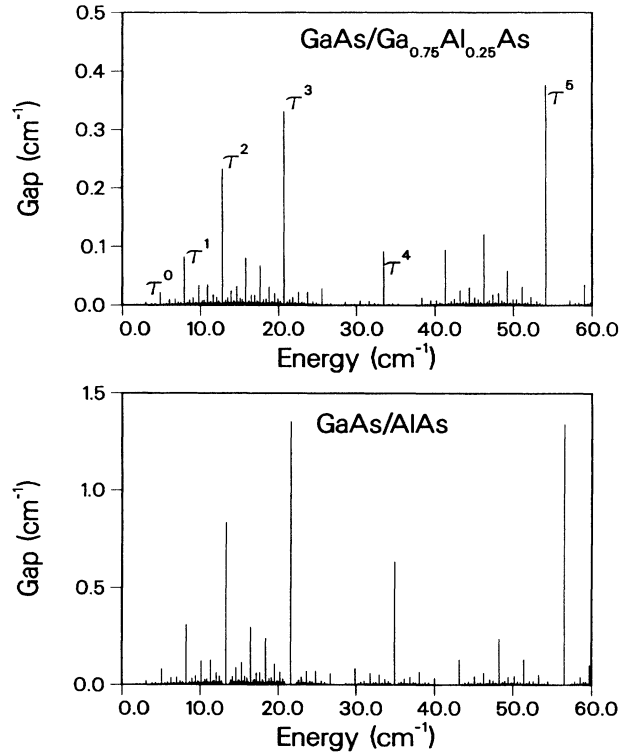


FIG. 2. Frequency gaps vs midgap frequency for the 12th-generation Fibonacci superlattices (with periodic boundary conditions) described in the text.

TABLE I. The main peaks in the Raman spectrum of the Fibonacci superlattice: ω_p^\pm ($p = -1, 0, 1, 2, 3$) is defined in Eq. (7) and $\omega_B = \bar{v}q$ is the Brillouin frequency. $\omega_0 = 9.75 \text{ cm}^{-1}$ with d calculated from the nominal layer widths.

	Peak frequency (cm^{-1})									
	ω_{-1}^-	ω_{-1}^+	ω_0^-	ω_0^+	ω_1^-	ω_1^+	ω_2^-	ω_2^+	ω_3^-	ω_3^+
457.9-nm excitation ($\omega_B = 3.25 \text{ cm}^{-1}$) ^a										
Theory	2.8	9.3	6.5	13.0	12.5	19.0	22.2	28.7	38.0	44.5
Expt.	2.9	9.8		12.3	12.3	18.7	21.7	28.2	37.6	43.6
647.1-nm excitation ($\omega_B = 1.85 \text{ cm}^{-1}$)										
Theory	4.2	7.9	7.9	11.6	14.0	17.7	23.9	27.6	39.5	43.2
Expt.		7.5	7.5		13.8	17.2	23.5	27.3	39.0	42.5
676.4-nm excitation ($\omega_B = 1.75 \text{ cm}^{-1}$)										
Theory	4.3	7.8	8.0	11.5	14.1	17.6	24.0	27.5	39.6	43.1
Expt.		7.9	7.9	11.3	13.7			27.8		

^aExperimentally, $\omega_B = 3.3 \pm 0.5 \text{ cm}^{-1}$.

reciprocal lattice perpendicular to the Fibonacci superlattice. $S(k_{n,m})$ becomes small as either $k_{n,m}$ or $Z_{n,m}$ gets large and, for $d_A/d_B \approx \tau$, achieves its maximum values when n and m are neighboring Fibonacci numbers,^{4,5,8} so that $k_{F_{p-1}, F_p} \equiv k_p = 2\pi\tau^p/d$ while (for $d_A/d_B \equiv \tau$) $Z_{F_{p-1}, F_p} \equiv Z_p = \pi\tau^{1-p}/(1+\tau^{-2})$. The current situation may be contrasted with the case where interval A is composed entirely of material 1 and interval B is compared entirely of material 2, where

$$|S(k_{n,m})|^2 = \left| \frac{2\tau^2 \sin(Z_{n,m}\tau^{-1}) \sin(k_{n,m}d_A/2)}{k_{n,m}Z_{n,m}d} \right|^2. \quad (6)$$

In the case of Eq. (5), $|S(k_{n,m})|^2$ is largest for $k_{n,m} = k_p$ with $p=0,1,2,3$. In the case of Eq. (6), the individual layers are thicker, in units of d , and hence $|S(k_{n,m})|$ and $|P(k_{n,m})|$ drop off less quickly as Z increases but more quickly as $k_{n,m}$ increases. Correspondingly, the most prominent features of the Raman spectra in this investigation occur at $\omega_B = \omega_0 q$ with $\omega_0 = 2\pi\bar{v}/d$, and at

$$\omega = \omega_p^\pm \equiv |\omega_0\tau^p \pm \omega_B| \quad (7)$$

with $p=0,1,2,3$ (see Fig. 1 and Table I) whereas in the case of Ref. 8 they occurred at $p = -1, 0, 1$, and 2.

The gaps in the phonon spectrum resulting from differences in the sound velocity of the two semiconductors may be estimated by treating the sound-velocity difference perturbatively. The Fourier transform of $v^2(\xi)$ is

$$(v_2^2 - v_1^2) \sum_{n,m} \delta(k - k_{n,m}) S(k_{n,m}) + \bar{v}^2 \delta(k).$$

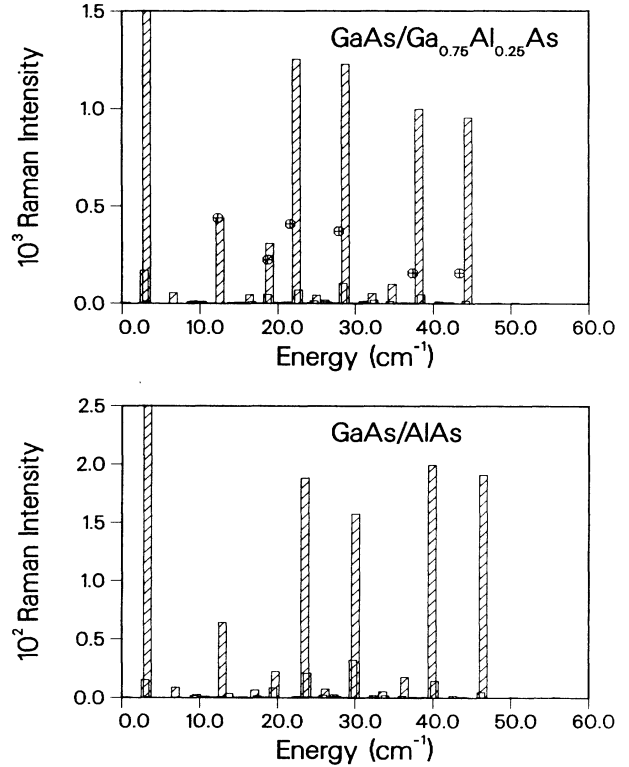


FIG. 3. Raman spectra for the 12th-generation Fibonacci superlattices described in the text calculated directly from Eq. (1). Here $P_{\text{AlAs}} \approx 0.1P_{\text{GaAs}}$, with $P_{\text{Ga}_{1-x}\text{Al}_x\text{As}}$ taken as a linear function of x . These results are for the high-temperature limit ($k_B T \gg \hbar\omega$) and the Brillouin peak intensity is off scale. The Raman intensity units are arbitrary but the same for the two panels. Experimental points (\oplus) are normalized to the 12.3- cm^{-1} peak.

The component at wave vector $k_{n,m}$ couples degenerate phonon modes at $q = \pm k_{n,m}/2$. Including only these two modes¹⁷ in Eq. (2) and using Eq. (5) gives gaps centered at $\omega_{n,m} \equiv \bar{v}k_{n,m}/2$ and of magnitude

$$\Delta_{n,m} = \left| \frac{v_2 - v_1}{\bar{v}} \right| \frac{\omega_0 \tau^2}{\pi} \left| \frac{\sin(k_{n,m} d_2 / 2) \sin(Z_{n,m})}{Z_{n,m}} \right| \leq \left| \frac{v_2 - v_1}{\bar{v}} \right| \frac{\omega_0 \tau^2}{\pi}. \quad (8)$$

Note that the maximum gap is proportional to the velocity difference and inversely proportional to the layer thicknesses. In Fig. 2 we show the gaps calculated exactly from Eq. (2) for $x=0.25$ and 1.0 by applying periodic boundary conditions after 12 generations, and these are in excellent agreement with the approximate expression [Eq. (8)]. For $x=0.25$ the maximum gap is 0.38 cm^{-1} , which is smaller than our experimental frequency resolution. Note that the largest gaps occur for $k_{n,m} = k_p$, as expected, and thus at $\omega_{n,m} = \omega_0 \tau^p / 2$. The smallness of the gaps means that corrections from velocity differences for the frequencies of features in the Raman spectrum are negligible, at least for $x=0.25$. However, as recently emphasized by Jusserand *et al.*¹³ for

the periodic case, substantial corrections do occur for the intensities of the spectral features. In Fig. 3 we show Raman spectra calculated from Eq. (1) without further approximation, for $x=0.25$ and 1.0. The intensity corrections depend on details of the sample geometry and on P_1/P_2 . They are most evident in the asymmetry of the doublets separated by $2\omega_B$ but, at least for $x=0.25$, these asymmetries are not large enough that we can make a useful comparison between theory and experiment. The intensity histogram of Fig. 3 assumes sharp step-function boundaries. The observed intensities, normalized to the experimental peak at 12.3 cm^{-1} , are shown as circled crosses. The experimental intensities fall off more rapidly and this can be attributed to interface broadening effects. Jusserand *et al.*¹⁸ have modeled this by assuming that the interface extends over several monolayers, giving rise to a partial error-function-like profile. Using their model, our data is consistent with an interface broadening of about four monolayers. However, there are several effects (e.g., interface roughness, local thickness fluctuations, and atomic diffusion) that can result in interface broadening and the model does not distinguish between these effects. Figure 3 also emphasizes that the Raman intensity for the alloy case ($x=0.25$) studied here is an order of magnitude weaker than in the GaAs-AlAs ($x=1.0$) case.⁹

- ¹D. Shtetman, I. Bloch, D. Gratias, and J. W. Cahn, Phys. Rev. Lett. **53**, 1951 (1984).
²D. Levine and P. J. Steinhardt, Phys. Rev. Lett. **53**, 2477 (1984).
³V. Elser and C. L. Henley, Phys. Rev. Lett. **55**, 2883 (1985); P. Guyot and M. Audier, Philos. Mag. B **52**, L15 (1985); C. L. Henley and V. Elser, *ibid.* **53**, L59 (1986).
⁴R. Merlin, K. Bajema, R. Clarke, F.-Y. Juang, and P. K. Bhattacharya, Phys. Rev. Lett. **55**, 1768 (1985).
⁵J. Todd, R. Merlin, R. Clarke, K. M. Mohanty, and J. D. Axe, Phys. Rev. Lett. **57**, 1157 (1986).
⁶M. G. Karkut, J.-M. Triscone, D. Ariosa, and O. Fischer, Phys. Rev. B **34**, 4390 (1986).
⁷A. Behrooz, M. J. Burns, H. Deckman, D. Levine, B. Whitehead, and P. M. Chaikin, Phys. Rev. Lett. **57**, 368 (1986).
⁸M. W. C. Dharma-wardana, A. H. MacDonald, D. J. Lockwood, J.-M. Baribeau, and D. C. Houghton, Phys. Rev. Lett. **58**, 1761 (1987).
⁹K. Bajema and R. Merlin, Phys. Rev. B **36**, 4555 (1987).
¹⁰C. Colvard, T. A. Gant, M. V. Klein, R. Merlin, R. Fischer,

- H. Morkoc, and A. C. Gossard, Phys. Rev. B **31**, 2080 (1985); B. Jusserand and D. Paquet, in *Semiconductor Heterojunctions and Superlattices*, edited by N. Boccara, G. Allan, G. Bastard, M. Lannoo, and M. Voos (Springer, Berlin, 1986), and references therein.
¹¹We assume here that the relevant elastic constant may be taken to have the same value in GaAs and $\text{Ga}_{1-x}\text{Al}_x\text{As}$ so that the change in local sound velocity is due entirely to the change in mass density.
¹²S.-Y. Ren and W. A. Harrison, Phys. Rev. B **23**, 762 (1981).
¹³B. Jusserand, D. Paquet, F. Mollat, F. Alexandre, and G. Le Roux, Phys. Rev. B **35**, 2808 (1987).
¹⁴V. Elser, Acta Crystallogr. Sec. A **42**, 36 (1986).
¹⁵R. K. Zia and W. J. Dallas, J. Phys. A **18**, L341 (1985).
¹⁶A. H. MacDonald (unpublished).
¹⁷The Fourier-transform analysis is similar to that discussed in Refs. 10 and 13 for the periodic case. The approximation used should be valid for small velocity differences.
¹⁸B. Jusserand, F. Alexandre, D. Paquet, and G. Le Roux, Appl. Phys. Lett. **47**, 301 (1985).